Received: 31 May 2020 | Revised: 8 December 2020 | Accepted: 26 December 2020

DOI: 10.1002/ddr.21782

RESEARCH ARTICLE

DRUG DEVELOPMENT RESEARCH WILEY

In silico design and synthesis of N-arylalkanyl 2-naphthamides as a new class of non-purine xanthine oxidase inhibitors

Sheau Ling Ho[1†] | Ching-Ting Lin[2†] | Shoei-Sheng Lee[2]

[1]Department of Chemical & Materials Engineering, Chinese Culture University, Taipei, Taiwan

[2]School of Pharmacy, College of Medicine, National Taiwan University, Taipei, Taiwan

Correspondence
Shoei-Sheng Lee, School of Pharmacy, College of Medicine, National Taiwan University, Taipei 10050, Taiwan.
Email: shoeilee@ntu.edu.tw

Funding information
Ministry of Science and Technology, Taiwan, Grant/Award Number: MOST 103-2320-B-002-011-MY3

Abstract

A series of *N*-arylalkanyl 2-naphthamides (**Xa**∼**e**), which were predicted from virtual molecular docking on a built xanthine oxidase template as potential inhibitors, were synthesized. Their inhibitory activity against xanthine oxidase was assayed. Among these prepared, compounds **Xb** (IC_{50} 13.6 μM), **Xc** (IC_{50} 13.1 μM), and **Xd** (IC_{50} 12.5 μM) showed comparable inhibitory activity to allopurinol (IC_{50} 22.1 μM). The in vitro assay result correlated well with molecular docking scores, ΔG = −16.99, −17.66, and −17.13 Kcal/mol, respectively. On the potassium oxonate-induced hyperuricemic mice model, oral administration of **Xc**-**Ac** (40 mg/ Kg), the per-*O*-acetylated **Xc**, could reduce the blood uric acid level by 60% in comparison to the normal control group and is statistically significant ($p < .01$) while compared with the hyperuricemic mice group.

KEYWORDS
in vitro and in vivo assay, molecular docking, *N*-arylalkanyl naphthamides, synthesis, xanthine oxidase inhibitor

1 | INTRODUCTION

Xanthine oxidase (XO), a molybdenum-containing hydroxylase, is an important enzyme which catalyzes oxidative hydroxylation of purine substrates (hypoxanthine and xanthine) to produce uric acid and reactive oxygen species (ROS) (Hille, 2006). The excessive production or insufficient excretion of uric acid results in hyperuricemia, which is associated with gout and the risk factor of chronic renal disease, metabolic syndrome, diabetes, and cardiovascular disease (Rock, Kataoka, & Lai, 2013). XO inhibitors (XOIs) block the formation of uric acid from purine, which mainly occurs in intestine and liver, leading to lowering blood uric acid level (Pacher, Nivorozhkin, & Szabo, 2006). Thus, the development of XOIs has become one of the therapeutic approaches for treating hyperuricemia.

Allopurinol, an XOI, is the most commonly used anti-gout drug (Pacher et al., 2006). However, it might cause several serious side effects, including hypersensitivity reactions, Steven's Johnson syndrome, hepatitis, nephropathy, and 6-mercaptopurine toxicity (Robinson & Dalbeth, 2015). Therefore, exploration of potent XOIs void of side effects is in urgent need. Febuxostat, the first non-purine XOI with higher potency than allopurinol, was approved in 2009 for gout treatment (Kumar, Darpan, & Singh, 2011). Many research groups have synthesized various non-purine XOIs, such as 2-phenyl-1*H*-imidazoles (Chen et al., 2015; Zhang et al., 2018), 5-arylazotropolones (Saito, Kisen, Kumagai, & Ohta, 2018), and *N*-(9,-10-anthraquinone-2-carbonyl)amino acids (Zhang, Li, Yuan, Zhang, & Meng, 2018) (Figure 1). Additionally, many natural products like flavonoids, coumarins, and stilbenes (Cao, Pauff, & Hille, 2014; Cos et al., 1998; Lin et al., 2008; Pauff & Hille, 2009; Silva, Mira, Lima, & Manso, 1996) (Figure 1) also displayed XO inhibitory activity.

Five 1,4-benzodioxane type neolignans and one styrenyl caffeate (Figure 2), isolated from *Hyptis rhomboids*, had been reported as active XOIs (IC_{50} 0.6–39.5 μM) in our previous study (Tsai & Lee, 2014). These active natural products are too minor to proceed further studies, such as in vivo experiments. Thus, alternative approaches to supply such analogs are required.

To gain insights into the binding mode of these neolignans, molecular docking of these compounds into the built XO template

† Equal contribution.

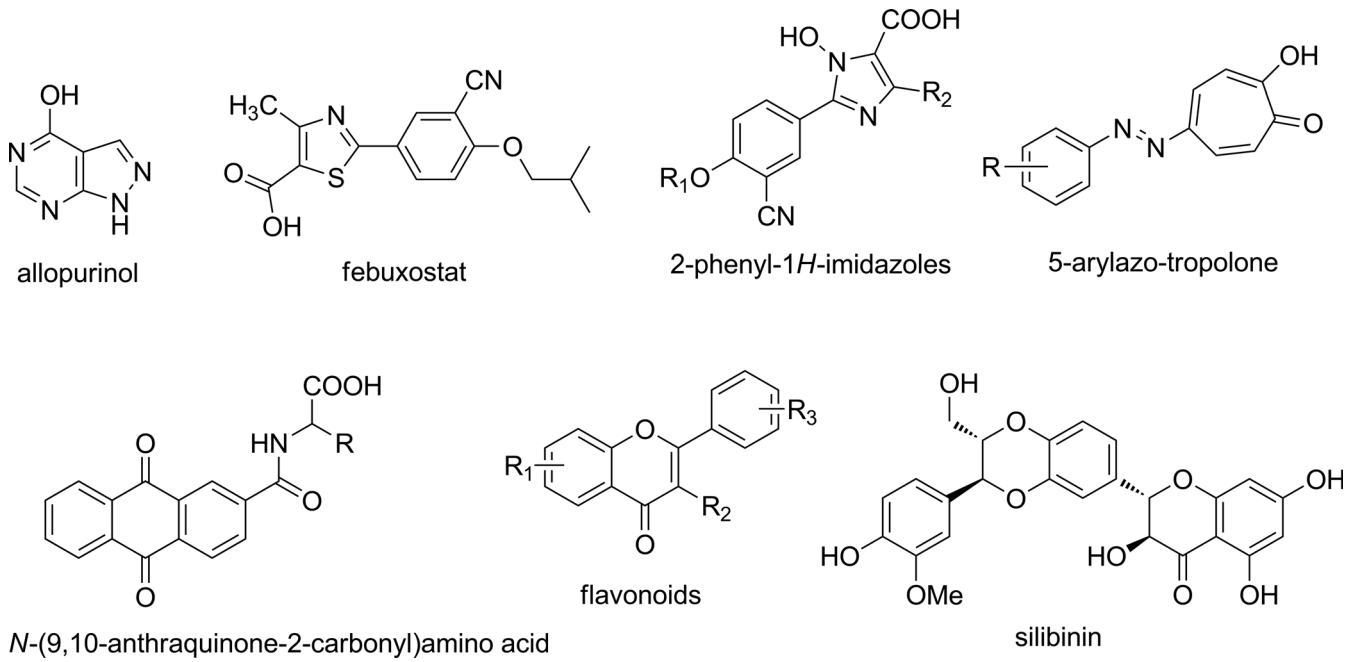

FIGURE 1 Structures of some synthetic and natural occurring xanthine oxidase inhibitors

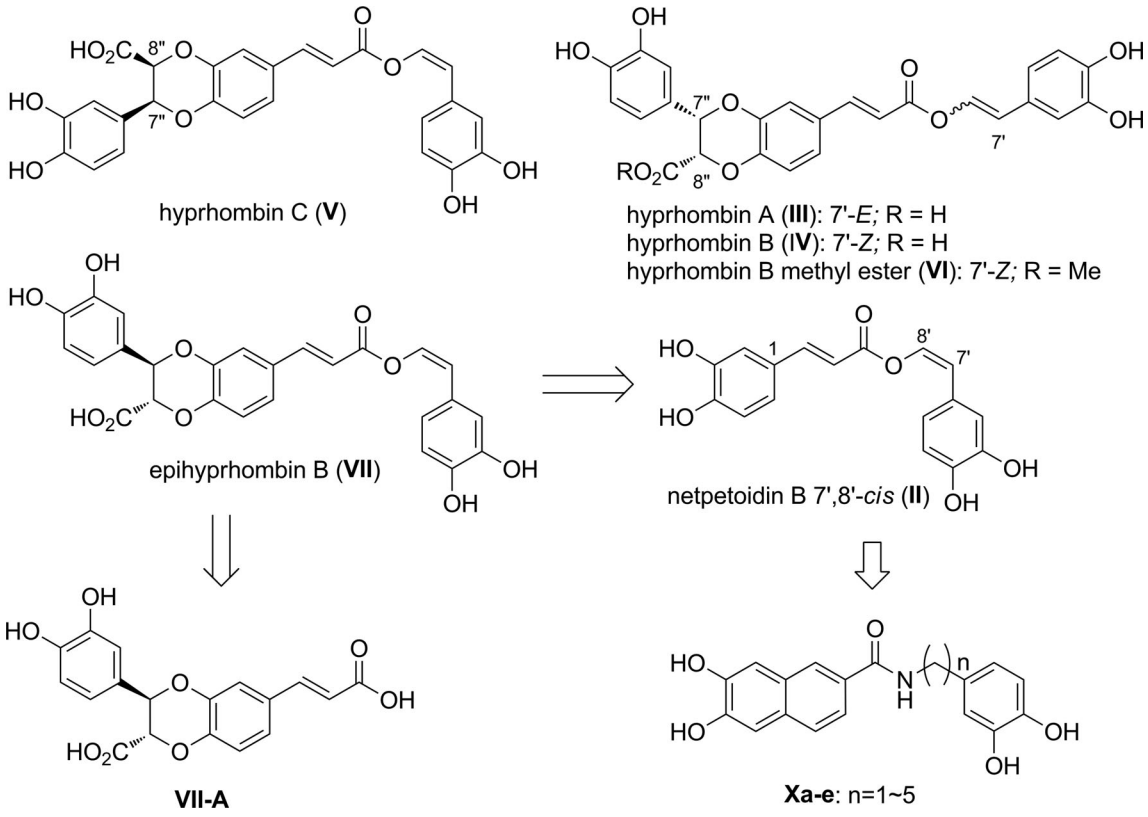

FIGURE 2 Structures of five 1,4-benzodioxane type neolignans and one styrenyl caffeate from *Hyptis rhomboids* and dereplication of **VII**

using MOE software was undertaken. The results showed that the docking scores of compounds **V**, **VII**, and **IV** with ΔG = −21.84, −21.46, −20.89 Kcal/mol, respectively, correlated well with the in vitro inhibition assays with the respective IC_{50} value of 0.6 ± 0.3 μM, 2.0 ± 0.1 μM, and 5.2 ± 0.5 μM, validating the built XO template (Ho, Tsai, Lin, Kim, & Lee, 2020).

Dereplication of the scaffold of epihyprhombin B (**VII**) (IC_{50} 2.0 μM) led to two parts, a 6-phenyl-benzo[*b*]-1,4-dioxane moiety

(**VII-A**) and a styryl phenylpropenoate moiety (**II**). Molecular docking of **VII-A** and **II** on XO template showed good docking score for both compounds (ΔG = −19.32 Kcal/mol, both). The 1,4-benzodioxane type neolignans such as **VII-A** have been synthesized via biomimetic approach through horseradish peroxidase catalyzed oxidative coupling of catechol containing phenylpropenoids, such as caffeic acid (Takahashi, Matsumoto, Ueda, Miyake, & Fukuyama, 2002). Besides the low yield, this approach gave isomeric products which raised purification issue, thus hampering the scale-up of the desired product. Consequently, the availability of such analogs from either synthesis or the nature is not practical. Netpetoidin B (**II**) is a relatively good XOI (IC_{50} 11.7 μM; cf 5.3 μM, allopurinol) (Tsai & Lee, 2014) but the styryl ester and conjugated double bond are potentially labile under stress (acid, base, light, air). Based on in silico molecular docking to XO template, a series of *N*-arylalkyl-2-naphthamides (**Xa—e**) was designed to overcome such structure drawback. The following describes the design, synthesis, and anti-XO activity of these target compounds.

2 | EXPERIMENTAL SECTION

2.1 | Molecular docking studies

2.1.1 | Data collection and preparation

The crystal structure of xanthine oxidase (XO) from bovine milk source was retrieved from the Protein Data Bank (PDB ID: 1FIQ). Xanthine oxidase is a homodimeric enzyme and each monomer consists of four components, including a molybdopterin cofactor (Mo-pt) center, a pair of spinach ferredoxin-like clusters [2Fe–2S], and one flavin adenine dinucleotide (FAD) cofactor (Enroth et al., 2000). Since the other three components are far from the active site, only the active site component, Mo-pt, was kept for molecular docking study. The active site of XO was constructed using the co-crystal structure of salicylate–xanthine oxidase complex as a reference.

The 2D structures of selected ligands were constructed using ChemBioDraw and converted into 3D structure using ChemBio3D software where energy minimization and molecular dynamics were undertaken.

2.1.2 | Docking simulation

All simulations were performed using Molecular Operating Environment (MOE), 2010.10 (Chemical Computing Group Inc., 1010 Sherbooke St. West, Suite #910, Montreal, QC, Canada, H3A 2R7, 2010). The partial atomic charges were assigned to XO using MMFF94x forcefield in MOE. The triangle matcher algorithm of the MOE software packages was selected to dock the identified hit compounds into the Mo-pt active site. Docking calculations were carried out using standard default variables. The RMSD was computed in terms of all the atoms in a protein backbone and the value was less than 0.6 Å, which is indicative of considerable structural similarity. The compounds were docked into the same binding site, and then the initial model was loaded into MOE working environment ignoring water molecules and heteroatoms. The structure with all the atoms shown was put in generalized born implicit solvated environment using the default setting. The dock scoring was implemented using London ΔG scoring function and enhanced by the Affinity ΔG refinement method. Refined poses were updated to satisfy the 3D spatial restraints of the specified conformations. The rotatable bonds were allowed and then the best 20 poses were retained to analyze their binding scores. Energy minimization was conducted through MMFF94x forcefield optimization by using a gradient cut-off value of 0.05 kcal/mol/Å for determining low energy conformations with the lowest energy geometry (Halgren, 1996). From the final list of these 20 docked conformations, the nondistorted one with the best docking score was chosen for further analysis.

2.2 | Chemistry

MP: MEL-TEMP; UV: U-2001 spectrophotometer; FT-IR: JASCO FT/IR-410; ^{1}H and ^{13}C NMR: Bruker AV 400 or Bruker AV-III 600 NMR spectrometer ($CDCl_3$, δ_H 7.24 and δ_C 77.0 ppm; methanol-d_4, δ_H 3.30 and δ_C 49.0 ppm; pyridine-d_5, δ_H 8.71 and δ_C 149.9 ppm; *J* in Hz); ESIMS: Bruker Esquire 200 ESI-ion trap spectrometer; HR-ESI-MS: Bruker micrOTOF orthogonal ESI-TOF mass spectrometer.

2.2.1 | Preparation of *N*-(3-[3,4-dimethoxyphenyl] propyl)-6,7-dimethoxy-2-naphthamide (28), a general procedure for preparing 26–30

The reaction mixture of the carboxylic acid **4** (250.3 mg, 1.08 mmol), the amine HCl salt **15** (284.2 mg, 1.23 mmol), triethylamine (166 μL), EDC (240.6 mg), and HOBt (164.0 mg) in CH_2Cl_2 – DMF (11 mL: 1 mL) was stirred at rt for 16 hr, then quenched with H_2O (120 mL). The resultant suspension was extracted with $CHCl_3$ (3 × 120 mL). The combined $CHCl_3$ layers were dried over anhy. Na_2SO_4 and concentrated under reduced pressure to give a residue, which was redissolved in $CHCl_3$ (60 mL) and the solution was washed sequentially with 5% citric acid (aq) (3 × 40 mL), sat. $NaHCO_3$ (aq) (3 × 60 mL), and brine (2 × 20 mL), dried over anhy. Na_2SO_4, and concentrated under reduced pressure to give a residue, which upon purification over a silica gel column (230–400 mesh, $CHCl_3$) yielded **28** (357.0 mg, 81%) as white amorphous solid.

UV (MeCN): λ_{max} (log ε) 332 (3.23), 282 (4.03), 244 nm (4.76).

IR (KBr): 3369, 3058, 2999, 2936, 2833, 1626, 1538, 1511, 1464, 1417, 1258, 1161, 1140, 1028, 1007, 858, 764, 735 cm^{-1}.

^{1}H NMR (400 MHz, $CDCl_3$): δ 7.96 (br s, 1H), 7.65 (d, *J* = 8.5 Hz, 1H), 7.57 (dd, *J* = 8.5, 1.7 Hz, 1H), 7.11 and 7.08 (each s, 2H), 6.77–6.71 (m, 3H), 6.32 (br t, 1H, D_2O exchangeable), 3.97 (s, 3H), 3.95 (s, 3H), 3.83 (s, 3H), 3.79 (s, 3H), 3.52 (q, *J* = 6.7 Hz, 2H), 2.67 (t, *J* = 7.4 Hz, 2H), 1.95 (quin, *J* = 7.0 Hz, 2H).

^{13}C NMR (100 MHz, $CDCl_3$): δ 167.6 (C), 150.7 (C), 149.9 (C), 148.9 (C), 147.3 (C), 134.1 (C), 130.8 (C), 130.1 (C), 128.3 (C), 126.5 (CH), 125.6 (CH), 121.8 (CH), 120.2 (CH), 111.6 (CH), 111.3 (CH), 106.9 (CH), 105.9 (CH), 55.8 (CH_3), 55.8 (CH_3), 55.8 (CH_3), 39.9 (CH_2), 33.2 (CH_2), 31.2 (CH_2).

MS (ESI): *m/z* 431.9 $[M+Na]^+$, 409.9 $[M+H]^+$.

HRMS (ESI) *m/z*: $[M+Na]^+$ calcd. for $C_{24}H_{27}NNaO_5$ 432.1781, found 432.1784.

N-*(3,4-Dimethoxybenzyl)-6,7-dimethoxy-2-naphthamide (**26**)*

Following the general procedure as described above, reacting **4** (47.5 mg, 0.20 mmol) with **7** (46.8 mg, 0.23 mmol) yielded **26** (67.6 mg, 87%) as yellowish amorphous solid.

UV (MeCN): λ_{max} (log ε) 334 (3.20), 284 (4.05), 244 nm (4.74).

IR (KBr): 3456, 1639, 1510, 1488, 1463, 1418, 1259, 1161, 1139, 750 cm^{-1}.

^{1}H NMR (400 MHz, $CDCl_3$): δ 8.15 (br s, 1H), 7.67 (s, 2H), 7.11 and 7.09 (each s, 2H), 6.91–6.89 (m, 2H), 6.81 (d, *J* = 8.6 Hz, 1H), 6.58 (br t, 1H, D_2O exchangeable), 4.59 (d, *J* = 5.3 Hz, 2H), 3.98 (s, 3H), 3.94 (s, 3H), 3.84 (s, 3H), 3.84 (s, 3H).

^{13}C NMR (100 MHz, $CDCl_3$): δ 167.5 (C), 150.8 (C), 150.0 (C), 149.1 (C), 148.4 (C), 130.9 (C), 130.8 (C), 129.8 (C), 128.3 (C), 126.6 (CH), 125.9 (CH), 121.9 (CH), 120.2 (CH), 111.3 (CH), 111.1 (CH), 106.9 (CH), 105.9 (CH), 55.8 (CH_3), 55.8 (CH_3), 44.0 (CH_2).

MS (ESI): *m/z* 403.9 $[M+Na]^+$, 381.9 $[M+H]^+$.

HRMS (ESI) *m/z*: $[M+Na]^+$ calcd. for $C_{22}H_{23}NNaO_5$ 404.1468, found 404.1464.

N-*(3,4-Dimethoxyphenethyl)-6,7-dimethoxy-2-naphthamide (**27**)*

Following the general procedure as described above, reacting **4** (51.4 mg, 0.2 mmol) with **8** (54.3 mg, 42 μL; 0.3 mmol) yielded **27** (78.4 mg, 90%) as white amorphous solid.

UV (MeCN): λ_{max} (log ε) 334 (3.14), 282 (4.00), 244 nm (4.72).

IR (KBr): 3561, 2959, 2835, 1639, 1509, 1489, 1464, 1418, 1259, 1160, 1141, 1028, 1006, 862, 764, 752 cm^{-1}.

^{1}H NMR (400 MHz, $CDCl_3$): δ 8.08 (br s, 1H), 7.68 (d, *J* = 8.5 Hz, 1H), 7.57 (dd, *J* = 8.5, 1.7 Hz, 1H), 7.12 and 7.10 (each s, 2H), 6.82 (d, *J* = 8.0 Hz, 1H), 6.78 (dd, *J* = 8.0, 1.6 Hz, 1H), 6.76 (d, *J* = 1.6 Hz, 1H), 6.26 (br t, 1H, D_2O exchangeable), 3.99 (s, 3H), 3.98 (s, 3H), 3.85 (s, 3H), 3.82 (s, 3H), 3.72 (q, *J* = 6.7 Hz, 2H), 2.89 (t, *J* = 6.8 Hz, 2H).

^{13}C NMR (100 MHz, $CDCl_3$): δ 167.7 (C), 150.8 (C), 150.1 (C), 149.0 (C), 147.7 (C), 131.5 (C), 130.9 (C), 130.0 (C), 128.4 (C), 126.6 (CH), 125.9 (CH), 121.7 (CH), 120.7 (CH), 111.9 (CH), 111.4 (CH), 106.9 (CH), 106.0 (CH), 55.9 (CH_3), 55.8 (CH_3), 41.3 (CH_2), 35.3 (CH_2).

MS (ESI): *m/z* 417.9 $[M+Na]^+$, 395.9 $[M+H]^+$.

HRMS (ESI) *m/z*: $[M+Na]^+$ calcd. for $C_{23}H_{25}NNaO_5$ 418.1625, found 418.1622.

N-*(4-[3,4-Dimethoxyphenyl]butyl)-6,7-dimethoxy-2-naphthamide (**29**)*

Following the general procedure as described above, reacting **4** (17.0 mg, 73 μmol) with **19** (20.0 mg, 78 μmol) yielded **29** (23.5 mg, 85%) as viscous liquid.

UV (MeCN): λ_{max} (log ε) 334 (3.23), 282 (4.08), 244 nm (4.82).

IR (KBr): 3390, 3000, 2934, 2855, 2834, 1627, 1537, 1510, 1463, 1438, 1417, 1257, 1247, 1161, 1140, 1028, 1007, 860, 772 cm^{-1}.

^{1}H NMR (400 MHz, $CDCl_3$): δ 8.11 (br s, 1H), 7.69 (d, *J* = 8.5 Hz, 1H), 7.63 (dd, *J* = 8.5, 1.7 Hz, 1H), 7.14 and 7.11 (each s, 2H), 6.77 (d, *J* = 8.2 Hz, 1H), 6.71 (dd, *J* = 8.2, 1.8 Hz, 1H), 6.69 (d, *J* = 1.8 Hz, 1H), 6.24 (br t, 1H, D_2O exchangeable), 3.99 (s, 3H), 3.97 (s, 3H), 3.84 (s, 3H), 3.83 (s, 3H), 3.50 (q, *J* = 6.6 Hz, 2H), 2.60 (t, *J* = 7.2 Hz, 2H), 1.73–1.66 (m, 4H).

^{13}C NMR (100 MHz, $CDCl_3$): δ 167.7 (C), 150.8 (C), 150.0 (C), 148.8 (C), 147.1 (C), 134.7 (C), 130.8 (C), 130.2 (C), 128.4 (C), 126.6 (CH), 125.8 (CH), 121.8 (CH), 120.1 (CH), 111.6 (CH), 111.1 (CH), 106.9 (CH), 106.0 (CH), 55.9 (CH_3), 55.9 (CH_3), 55.9 (CH_3), 55.8 (CH_3), 39.9 (CH_2), 35.1 (CH_2), 29.2 (CH_2), 28.9 (CH_2).

MS (ESI): *m/z* 445.9 $[M+Na]^+$, 423.9 $[M+H]^+$.

HRMS (ESI) *m/z*: $[M+Na]^+$ calcd. for $C_{25}H_{29}NNaO_5$ 446.1938, found 446.1930.

N-*(5-[3,4-Dimethoxyphenyl]pentyl)-6,7-dimethoxy-2-naphthamide (**30**)*

Following the general procedure as described above, reacting **4** (18.3 mg, 78 μmol) with **25** (22.4 mg, 86 μmol) yielded **30** (12.8 mg, 37%) as viscous liquid.

UV (MeCN): λ_{max} (log ε) 332 (3.15), 282 (3.93), 242 nm (4.69).

IR (KBr): 3380, 3000, 2933, 2854, 1627, 1540, 1508, 1463, 1417, 1258, 1248, 1161, 1140, 1028, 1007, 857, 771 cm^{-1}.

^{1}H NMR (400 MHz, $CDCl_3$): δ 8.12 (br s, 1H), 7.70 (d, *J* = 8.4 Hz, 1H), 7.62 (d, *J* = 8.4 Hz, 1H), 7.15 and 7.11 (each s, 2H), 6.75 (d, *J* = 8.6 Hz, 1H), 6.70–6.68 (m, 2H), 6.22 (br. s, 1H, D_2O exchangeable), 4.00 (s, 3H), 3.98 (s, 3H), 3.84 (s, 3H), 3.81 (s, 3H), 3.48 (m, 2H), 2.56 (t, *J* = 7.7 Hz, 2H), 1.67–1.63 (m, 4H), 1.47–1.39 (m, 2H).

^{13}C NMR (100 MHz, $CDCl_3$): δ 167.7 (C), 150.8 (C), 150.1 (C), 148.7 (C), 147.0 (C), 135.0 (C), 130.8 (C), 130.2 (C), 128.4 (C), 126.6 (CH), 125.8 (CH), 121.8 (CH), 120.1 (CH), 111.7 (CH), 111.1 (CH), 107.0 (CH), 106.0 (CH), 55.9 (CH_3), 55.9 (CH_3), 55.8 (CH_3), 40.1 (CH_2), 35.3 (CH_2), 31.2, (CH_2), 29.6 (CH_2), 26.5 (CH_2).

MS (ESI): *m/z* 459.9 $[M+Na]^+$, 437.9 $[M+H]^+$.

HRMS (ESI) *m/z*: $[M+Na]^+$ calcd. for $C_{26}H_{31}NNaO_5$ 460.2094, found 460.2089.

2.2.2 | Preparation of *N*-(3-[3,4-Dihydroxyphenyl] propyl)-6,7-dihydroxy-2-naphthamide (Xc), a general procedure for preparing *N*-arylalkanyl 2-naphthamides (Xa—Xe)

To a solution of **28** (151.7 mg) in CH_2Cl_2 (16 mL) was added a solution of boron tribromide in CH_2Cl_2 (1.0 M, 3 mL) dropwise at 0 °C. The reaction mixture was stirred at 0 °C for 1 hr, then quenched by adding MeOH (20 mL) dropwise and stirred for 1 hr, concentrated under reduced pressure to give a residue, which was added H_2O (5 mL) and the insoluble was collected by filtration. The filtrate was passed

through an Amberlite XAD-II column (20–60 mesh, pore radius 90 Å), eluted by H_2O and MeOH in sequence. The insoluble part and the residue of the MeOH eluate after evaporation were combined and then separated over a Sephadex LH-20 column (57 cm × 1.5 cm, MeOH-$CHCl_3$ 7:3) to give **Xc** (129.7 mg, 99%) as colorless amorphous solid.

UV (MeOH): λ_{max} (log ε) 288.0 (4.03), 248.0 nm (4.74).

IR (KBr): 3402, 1620, 1602, 1525, 1431, 1362, 1319, 1251, 1202, 1116, 864, 764, 639 cm^{-1}.

^1H NMR (400 MHz, CD_3OD): δ 8.02 (br s, 1H), 7.60 (d, J = 8.6 Hz, 1H), 7.57 (dd, J = 8.6, 1.6 Hz, 1H), 7.20 and 7.13 (each s, 2H), 6.67 (d, J = 8.1 Hz, 1H), 6.66 (d, J = 2.0 Hz, 1H), 6.54 (dd, J = 8.1, 2.0 Hz, 1H), 3.40 (t, J = 7.1 Hz, 2H), 2.56 (t, J = 7.4 Hz, 2H), 1.89 (quintet, J = 7.5 Hz, 2H).

^{13}C NMR (100 MHz, CD_3OD): δ 170.8 (C), 149.6 (C), 148.5 (C), 146.2 (C), 144.3 (C), 134.7 (C), 132.6 (C), 130.2 (C), 129.8 (C), 127.0 (CH), 126.8 (CH), 122.2 (CH), 120.7 (CH), 116.5 (CH), 116.3 (CH), 111.5 (CH), 110.3 (CH), 40.9 (CH_2), 33.8 (CH_2), 32.5 (CH_2).

MS (ESI): m/z 351.7 $[M-H]^-$.

HRMS (ESI) m/z: $[M-H]^-$ calcd. for $C_{20}H_{18}NO_5$ 352.1190, found 352.1204.

N-*(3,4-Dihydroxybenzyl)-6,7-dihydroxy-2-naphthamide (**Xa**)*

Following the general procedure as described above, **Xa** (29.7 mg, 98%) was obtained by reacting **26** (35.6 mg) with BBr_3 in CH_2Cl_2 (1.0 M, 0.8 mL) as white amorphous solid.

UV (MeOH): λ_{max} (log ε) 288.0 (4.09), 248.0 nm (4.78).

IR (KBr): 3485, 3413, 3341, 3293, 3069, 1593, 1578, 1519, 1491, 1428, 1366, 1288, 1265, 1206, 1156, 1115, 996, 903, 869, 825, 766, 638, 597, 515, 476 cm^{-1}.

^1H NMR (400 MHz, CD_3OD): δ 8.10 (d, J = 0.9 Hz, 1H), 7.64 (dd, J = 8.5, 1.7 Hz, 1H), 7.60 (d, J = 8.5 Hz, 1H), 7.19 and 7.13 (each s, 2H), 6.82 (d, J = 1.8 Hz, 1H), 6.73 (d, J = 8.1 Hz, 1H), 6.69 (dd, J = 8.1, 1.8 Hz, 1H), 4.45 (s, 2H).

^{13}C NMR (100 MHz, CD_3OD): δ 170.6 (C), 149.7 (C), 148.6 (C), 146.4 (C), 145.5 (C), 132.6 (C), 131.9 (C), 130.1 (C), 129.9 (C), 127.1 (CH), 127.0 (CH), 122.3 (CH), 120.1 (CH), 116.3 (CH), 115.8 (CH), 111.5 (CH), 110.3 (CH), 44.2 (CH_2).

MS (ESI): m/z 323.8 $[M-H]^-$.

HRMS (ESI) m/z: $[M-H]^-$ calcd. for $C_{18}H_{14}NO_5$ 324.0877, found 324.0869.

N-*(3,4-Dihydroxyphenethyl)-6,7-dihydroxy-2-naphthamide (**Xb**)*

Following the general procedure as described above, **Xb** (13.9 mg, 84%) was obtained by reacting **27** (19.2 mg) with BBr_3 in CH_2Cl_2 (1.0 M, 0.4 mL) as amorphous solid.

UV (MeOH): λ_{max} (log ε) 288.0 (3.99), 248.0 nm (4.67).

IR (KBr): 3332, 1620, 1526, 1455, 1422, 1360, 1320, 1249, 1198, 1117, 1058, 861, 806, 762, 611 cm^{-1}.

^1H NMR (400 MHz, CD_3OD): δ 8.03 (br s, 1H), 7.60 (d, J = 8.5 Hz, 1H), 7.57 (dd, J = 8.5, 1.6 Hz, 1H), 7.18 and 7.13 (each s, 2H), 6.70 (d, J = 2.0 Hz, 1H), 6.69 (d, J = 8.0 Hz, 1H), 6.58 (dd, J = 8.0, 2.0 Hz, 1H), 3.54 (t, J = 7.7 Hz, 2H), 2.77 (t, J = 7.7 Hz, 2H).

^{13}C NMR (100 MHz, CD_3OD): δ 170.8 (C), 149.7 (C), 148.6 (C), 146.3 (C), 144.8 (C), 132.6 (C), 132.3 (C), 130.2 (C), 129.9 (C), 127.0 (CH), 126.8 (CH), 122.2 (CH), 121.1 (CH), 117.0 (CH), 116.4 (CH), 111.4 (CH), 110.3 (CH), 43.1 (CH_2), 36.1 (CH_2).

MS (ESI): m/z 337.8 $[M-H]^-$.

HRMS (ESI) m/z: $[M-H]^-$ calcd. for $C_{19}H_{16}NO_5$ 338.1034, found 338.1030.

N-*(4-[3,4-Dihydroxyphenyl]butyl)-6,7-dihydroxy-2-naphthamide (**Xd**)*

Following the general procedure as described above, **Xd** (7.5 mg, 60%) was yielded by reacting **29** (14.5 mg) with BBr_3 in CH_2Cl_2 (1.0 M, 0.3 mL) as amorphous solid.

UV (MeOH): λ_{max} (log ε) 288.0 (4.00), 248.0 nm (4.70).

IR (KBr): 3363, 2937, 1618, 1602, 1523, 1430, 1359, 1321, 1250, 1202, 1116, 863, 758, 611 cm^{-1}.

^1H NMR (400 MHz, CD_3OD): δ 8.05 (br s, 1H), 7.59–7.58 (m, 2H), 7.19 and 7.13 (each s, 2H), 6.65 (d, J = 8.0 Hz, 1H), 6.62 (d, J = 2.0 Hz, 1H), 6.50 (dd, J = 8.0, 2.0 Hz, 1H), 3.40 (t, J = 6.6 Hz, 2H), 2.51 (t, J = 6.8 Hz, 2H), 1.64 (m, 4H).

^{13}C NMR (100 MHz, CD_3OD): δ 170.8 (C), 149.6 (C), 148.6 (C), 146.1 (C), 144.2 (C), 135.3 (C), 132.6 (C), 130.2 (C), 129.9 (C), 127.0 (CH), 126.8 (CH), 122.2 (CH), 120.7 (CH), 116.5 (CH), 116.2 (CH), 111.4 (CH), 110.3 (CH), 40.9 (CH_2), 35.9 (CH_2), 30.3 (CH_2), 30.1 (CH_2).

MS (ESI): m/z 365.8 $[M-H]^-$.

HRMS (ESI) m/z: $[M-H]^-$ calcd. for $C_{21}H_{20}NO_5$ 366.1347, found 366.1342.

N-*(5-[3,4-Dihydroxyphenyl]pentyl)-6,7-dihydroxy-2-naphthamide (**Xe**)*

Following the general procedure as described above, **Xe** (3.0 mg, 51%) was obtained by reacting **30** (6.8 mg) with BBr_3 in CH_2Cl_2 (1.0 M, 0.15 mL) as amorphous solid.

UV (MeOH): λ_{max} (log ε) 290.0 (3.85), 248.0 nm (4.47).

IR (KBr): 3375, 2934, 2857, 1618, 1524, 1430, 1363, 1317, 1251, 1202, 1116, 1058, 1016, 864, 766, 639 cm^{-1}.

^1H NMR (400 MHz, CD_3OD): δ 8.04 (br s, 1H), 7.59–7.58 (m, 2H), 7.19 and 7.13 (each s, 2H), 6.63 (d, J = 8.0 Hz, 1H), 6.60 (d, J = 2.0 Hz, 1H), 6.48 (dd, J = 8.0, 2.0 Hz, 1H), 3.38 (t, J = 7.2 Hz, 2H), 2.48 (t, J = 7.4 Hz, 2H), 1.69–1.58 (m, 4H), 1.44–1.37 (m, 2H).

^{13}C NMR (100 MHz, CD_3OD): δ 170.9 (C), 149.6 (C), 148.6 (C), 146.0 (C), 144.1 (C), 135.5 (C), 132.6 (C), 130.3 (C), 129.9 (C), 127.1 (CH), 126.8 (CH), 122.2 (CH), 120.7 (CH), 116.5 (CH), 116.2 (CH), 111.5 (CH), 110.3 (CH), 41.0 (CH_2), 36.1 (CH_2), 32.6 (CH_2), 30.4 (CH_2), 27.6 (CH_2).

MS (ESI): m/z 379.8 $[M-H]^-$.

HRMS (ESI) m/z: $[M-H]^-$ calcd. for $C_{22}H_{22}NO_5$ 380.1503, found 380.1509.

2.2.3 | *N*-(3-[3,4-Diacetoxyphenyl]propyl)-6,7-diacetoxy-2-naphthamide (31)

The solution of **Xc** (99.5 mg) in pyridine (3 mL) and acetic anhydride (1.5 mL) was stirred at rt for 16 hr, quenched with abs. EtOH (3 mL),

concentrated under reduced pressure to give a residue, which was purified over a silica gel column (230–400 mesh, $CHCl_3$) to give **31** (143.2 mg, 98%) as colorless amorphous solid.

UV (MeCN): λ_{max} (log ε) 280 (3.87), 232 nm (4.79).

IR (KBr): 3424, 2936, 1768, 1643, 1540, 1505, 1471, 1427, 1371, 1210, 1110, 1012, 917, 764, 748 cm^{-1}.

^1H NMR (600 MHz, $CDCl_3$): δ 8.12 (br s, 1H), 7.80 (d, J = 8.6 Hz, 1H), 7.73 (dd, J = 8.6, 1.6 Hz, 1H), 7.71 and 7.66 (each s, 2H), 7.08 (dd, J = 8.2, 1.6 Hz, 1H), 7.07 (d, J = 8.2 Hz, 1H), 7.03 (d, J = 1.6 Hz, 1H), 6.25 (br. t, 1H, D_2O exchangeable), 3.53 (q, J = 6.8 Hz, 2H), 2.72 (t, J = 7.5 Hz, 2H), 2.33 and 2.33 (each s, 6H), 2.26 and 2.25 (each s, 6H), 1.99 (quin, J = 7.1 Hz, 2H).

^{13}C NMR (150 MHz, $CDCl_3$): δ 168.4 (C), 168.4 (C), 168.3 (C), 168.3 (C), 167.1 (C), 142.3 (C), 141.9 (C), 141.6 (C), 140.3 (C), 140.2 (C), 132.9 (C), 132.3 (C), 130.8 (C), 128.0 (CH), 126.7 (CH), 126.5 (CH), 124.1 (CH), 123.3 (CH), 123.3 (CH), 121.9 (CH), 120.8 (CH), 39.8 (CH_2), 32.9 (CH_2), 30.8 (CH_2), 20.7 (CH_3), 20.7 (CH_3), 20.6 (CH_3), 20.6 (CH_3).

MS (ESI): m/z 543.8 $[M+Na]^+$, 521.8 $[M+H]^+$.

HRMS (ESI) m/z: $[M+Na]^+$ calcd. for $C_{28}H_{27}NNaO_9$ 544.1578, found 544.1581.

2.3 | Xanthine oxidase inhibitory assay

The assay method for the prepared target compounds against XO activity was modified from a previous report (Khan, Ali, Gul, & Choudhary, 2008). To the corresponding well in a 96-well plate was added vehicle [10 μL, MeOH – H_2O or DMSO – H_2O 1:9 (vol/vol)] or sample in vehicle [10 μL, MeOH – H_2O (vol/vol) for netpetoidin B (**II**) and **Xa-e**; DMSO – H_2O 1:9 (vol/vol) for **28** and **31**], and 2 mM xanthine (Sigma) solution (60 μL). The reaction started when xanthine oxidase (30 μL, 0.2 U/mL) (EC 1.2.3.2, bovine milk, Sigma) was added. The produced uric acid was determined by measuring the absorbance at 290 nm on a Microplate spectrophotometer SPECTRAmax® PLUS (Molecular Devices) at 2 min intervals. The inhibitory percentage (%) of the test sample against XO was calculated by the following equation: inhibition (%) = $[1 - (A_{sample}/A_{control})] \times 100$, where $A_{control}$ and A_{sample} stand for the recorded absorbance value (A) of the blank and the test sample. The IC_{50} value was determined by the dose–response curve of five concentrations (0.5, 1, 5, 10, and 100 μg/mL) of each test sample in triplicate. Allopurinol (Synmosa Biopharma Corporation) whose IC_{50} values were found to be 22.1 ± 0.7 μM was used as a positive control.

2.4 | Evaluation of the in vivo efficacy

2.4.1 | Animal

Male ICR mice (4 weeks old) were purchased from the BioLASCO Taiwan, Co., Ltd (Taipei, Taiwan). Animals were allowed to adapt to the environment at least 1 week before experiments. They were housed at 20°C with a regular light/dark cycle, a standard fodder and water ad libitum during the study. The study protocol was approved by the Institutional Animal Care and Use Committee (IACUC), NTU (Approved no. IACUC No.20130383. MOST 103-2320-B-002-011-MY3).

2.4.2 | Potassium oxonate-induced hyperuricemic mice model (Kong, Yang, Ge, Wang, & Guo, 2004; Wu, Ruan, Zhang, Wang, & Zhang, 2014)

Blood was collected from the mice orbital sinus 1 day before experiments. Fodder, but not water, was withdrawn 1.5 hr prior to drug administration. In order to induce hyperuricemic status, potassium oxonate (250 mg/kg) was intraperitoneally injected 1 hr before administration of test compounds at 1st, 3rd, 5th, and 7th day. The test compounds (**28**, **31**) were suspended and allopurinol was dissolved in 15% Tween 80 (aq), then individually administered orally once per day. Blood (0.1 mL per mouse) was collected from the mouse orbital sinus 1 hr after final administration. All mice were sacrificed after the final blood collection.

2.4.3 | Measurement of plasma uric acid concentration

The uric acid concentration in mouse serum was measured by HPLC with the conditions modified from a previous report (Ingebretsen, Borgen, & Farstad, 1982). Each collected blood sample was allowed to clot at room temperature, centrifuged at 7000 × g for 10 min. The supernatant collected was treated with an equivalent volume of MeCN, votexed for 10 s, centrifuged at 10,000 × g for 10 min. The supernatant was filtered through 0.45 μm filter membrane. The filtrate was analyzed on an Agilent (Waldbronn, Germany) series 1100 HPLC, equipped with an analytical RP-18 column (Phenomenex Prodigy ODS-3, 250 × 4.6 mm, 5 μm) connected to a UV detector (Bruker, Rheinstetten, Germany). The delivery system [50 mM KH_2PO_4 (A), MeCN (B)] was as follows: 5% B/A for 10 min, 5% to 50% B/A in 10 min, 50% to 5% B/A in 10 min, all linear gradient; injection volume, 10 μL; flow rate, 0.5 mL/min; detection at 290 nm.

3 | RESULTS AND DISCUSSION

3.1 | Design of *N*-arylalkanyl-2-naphthamides as xanthine oxidase inhibitors

Structure–activity relationship of the active neolignans suggests that the presence of cinnamic acid moiety coupling with a *cis*-styryl moiety is an important structural feature for the inhibitory potency. The simplest approach to design target compounds derived from the styryl caffeate **II** was to replace the caffeic acid and styryl alcohol moieties by naphthoic acid and phenethylamine, respectively. Condensation of

TABLE 1 In vitro XO inhibition assay and computer assisted docking results of *N*-arylalkanyl 2-naphthamides, netpetoidin B (**II**), and allopurinol

				Number of ligand-receptor interaction							
				H-bond		n–π		π–π		Ionic	
Compd	ΔG_{calc} kcal/mol	Log *p*	IC_{50}[a] (μM)	T[b]	A[c]	T	A	T	A	T	A
Xa	−16.11	2.35	25.6 ± 0.4	3	1	3	3	1	1	0	0
Xb	−16.99	2.63	13.6 ± 1.0	3	2	4	1	1	1	0	0
Xc	−17.66	3.04	13.1 ± 0.4	4	2	3	3	1	1	0	0
Xd	−17.13	3.46	12.5 ± 1.9	4	2	3	3	1	1	0	0
Xe	−16.11	3.88	18.2 ± 0.7	2	1	2	1	1	1	0	0
28	−15.86	4.10	—[d]	2	2	1	0	1	1	0	0
31	−10.59	2.95	—[d]	1	1	2	1	0	0	0	0
II	−19.11	2.78	7.4 ± 0.2	4	2	1	1	1	1	0	0
allopurinol	−11.18	0.32	22.1 ± 0.7	3	3	1	1	1	1	0	0

[a]IC_{50}: the concentration of inhibitor required to produce 50% inhibition of XO (mean ± *SD*; *n* = 3).
[b]Total interaction number.
[c]Interaction number at the active site.
[d]Very poor solubility.

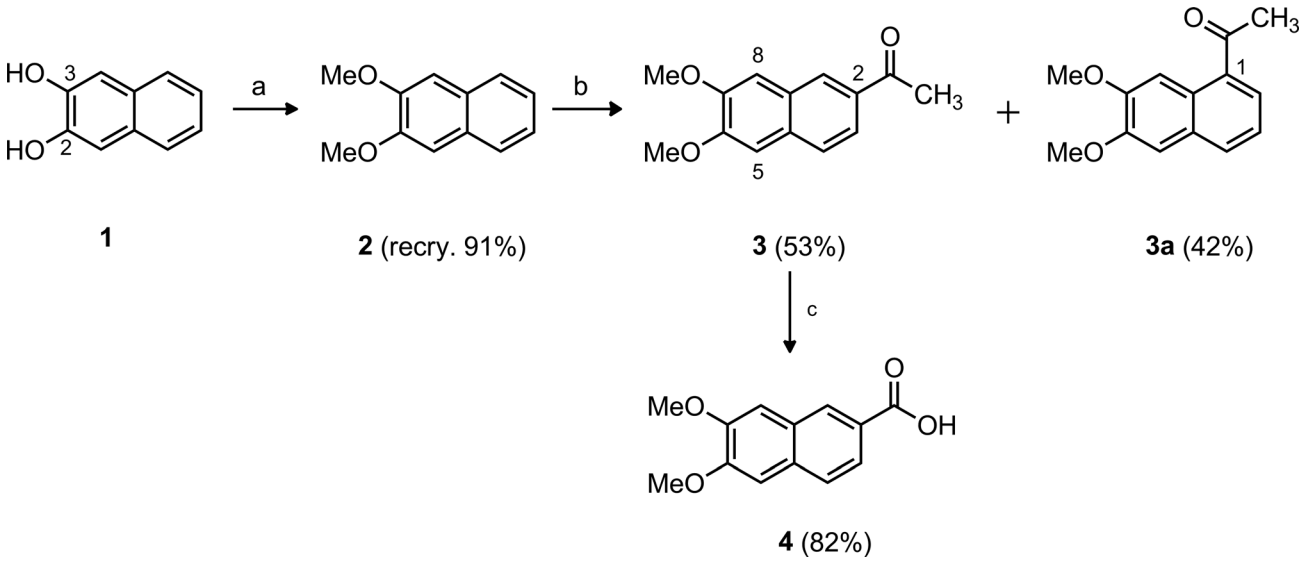

SCHEME 1 Preparation of 6,7-dimehtoxy-2-naphthoic acid (**4**): (a) Me_2SO_4, K_2CO_3, Me_2CO, reflux; (b) AcCl/$AlCl_3$, DCM, 0°C; (c) (i) Br_2, NaOH (aq); (ii) 6 M HCl

the carboxylic acids and the amines to form *N*-arylalkanyl 2-naphthamides (**Xa—e**) (Figure 2), which should be more bio-stable than the ester **II**. In silico molecular docking of **Xa—e** on XO template showed the docking scores around −17 Kcal/mol, of which **Xb-c** (n = 2–4; Figure 2) showed better binding affinity (Table 1).

3.2 | Synthesis of *N*-arylalkanyl-2-naphthamides

N-Arylalkanyl 2-naphthamides **Xa-e** were prepared as follows. The target **Xa-e** were prepared by coupling of 6,7-dimethoxy-2-naphthoic acid (**4**) with 3,4-dimethoxyphenyl-alkylamines (**7**, **8**, **15**, **19**, **25**), followed by per-*O*-demethylation.

The carboxylic acid **4** was prepared starting from 2,3-dihydroxy naphthalene. Per-*O*-methylation of 2,3-dihydroxynaphthalene (**1**) with dimethyl sulfate gave di-*O*-methylated product (**2**) (91% yield). Friedel-Crafts acylation of **2** with acetyl chloride/ $AlCl_3$ yielded 2-acetylated (**3**) (53% yield) and 1-acetylated (**3a**) (42% yield) products, both being separated by silica gel CC. Reaction of **3** with bromine in strong alkali, followed by acid workup, yielded 6,7-dimehtoxy-2-naphthoic acid (**4**) (82% yield) (Goksu, Kazaz, Sutbeyaz, & Secen, 2003) (Scheme 1).

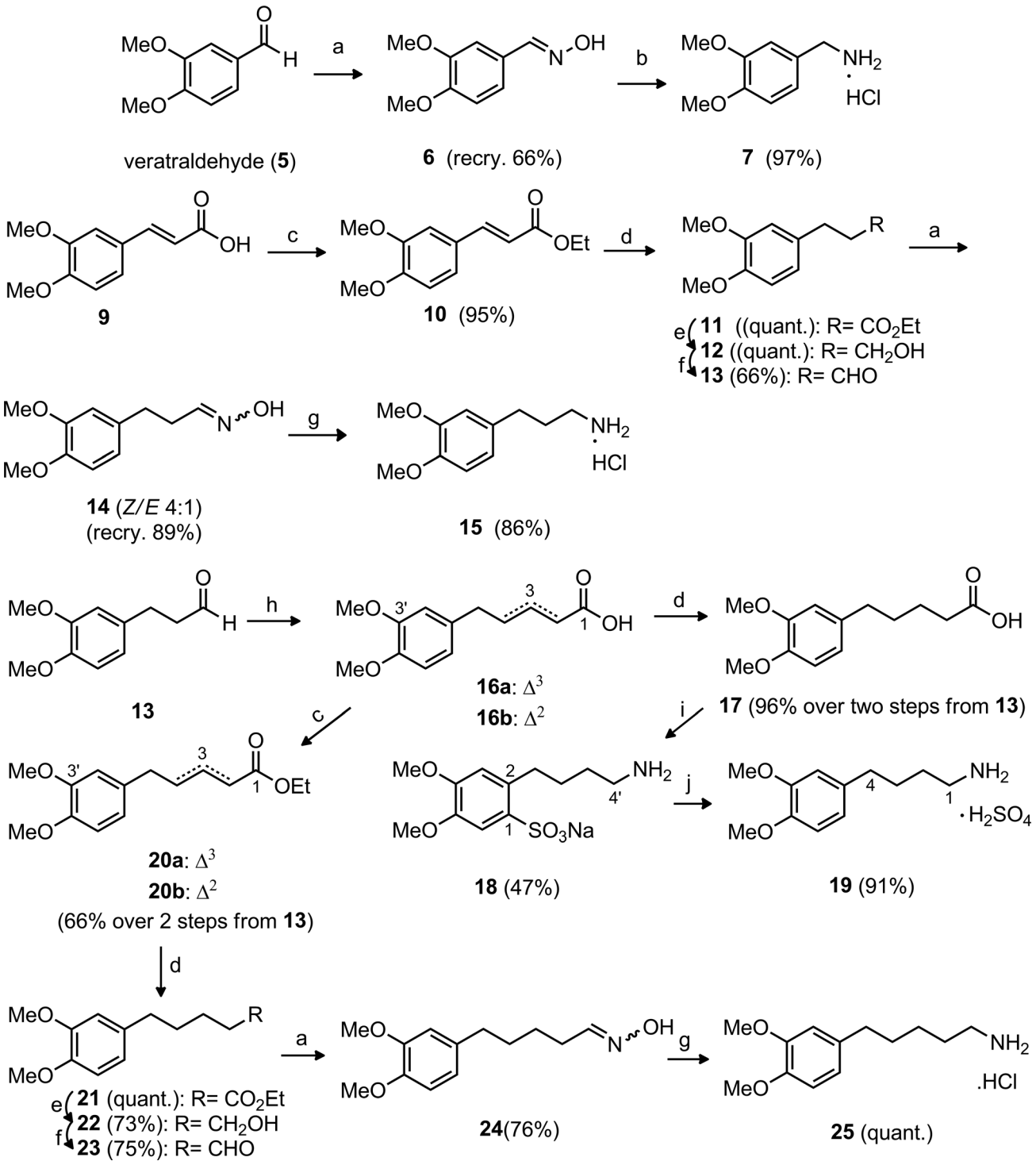

SCHEME 2 Preparation of 3,4-dimethoxyphenylalkanamines (**7**, **15**, **19**, **25**): (a) $NH_2OH{\cdot}HCl$, EtOH, rt; (b) H_2 (1 atm), 10% Pd/C, EtOH, conc. HCl, rt; (c) EtOH, H_2SO_4/reflux; (d) H_2 (1 atm), 10% Pd/C/EA, rt; (e) $LiALH_4$/THF, rt; (f) PCC, DCM, 0°C; (g) H_2 (1 atm), 10% Pd/C/MeOH, conc. HCl, rt; (h) $CH_2(CO_2H)_2$, py.-piperidine, reflux; (i) (i) NaN_3, H_2SO_4, $CHCl_3$; (ii) NaOH (aq); (j) 50% H_2SO_4 (aq)

3,4-Dimethoxybenzylamine hydrochloride (**7**) was prepared by reacting veratraldehyde (**5**) with hydroxylamine hydrochloride in the presence of sodium acetate (Soni et al., 2013) to yield oxime **6** (66%), followed by catalytic hydrogenation under acidic conditions (10% Pd/C-HCl) (97% yield) (Tsou et al., 2009). While 3-(3,4-dimethoxyphenyl)propylamine hydrochloride (**15**) was prepared starting from 3,4-dimethoxycinnamic acid (**9**). Esterification of **9** with ethanol/ H_2SO_4 (cat.) yielded the ethyl ester **10** (95% yield), which gave the alcohol **12** upon catalytic hydrogenation (10% Pd/C) (quant. yield) and subsequent LAH reduction (99% yield) (Lal, Ghosh, &

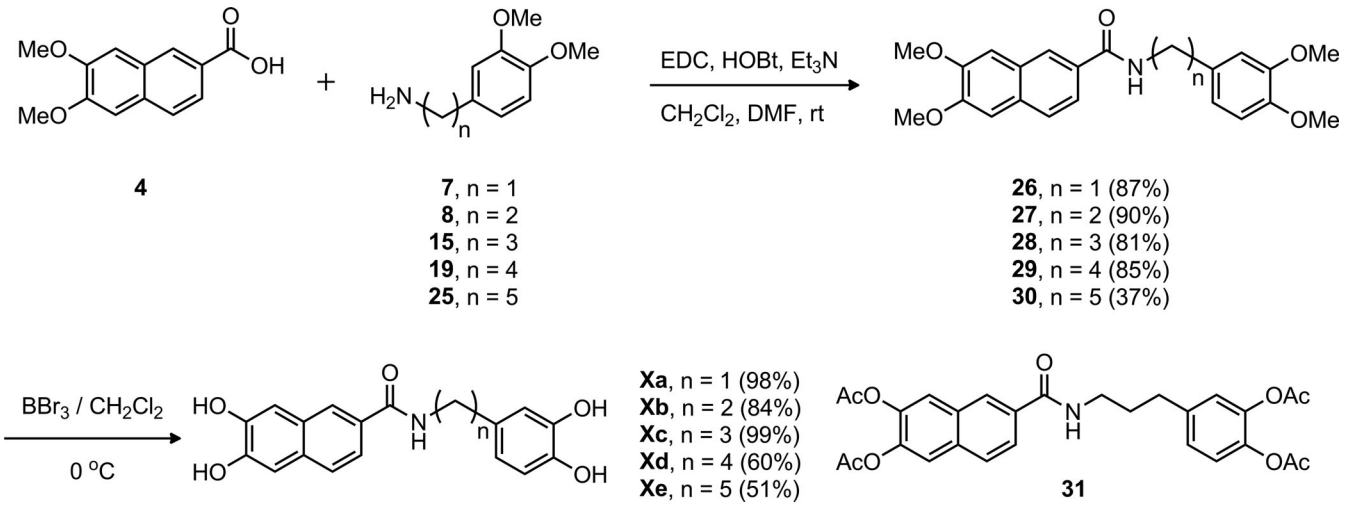

SCHEME 3 Preparation of *N*-arylalkanyl-2-naphthamides (**Xa-e**)

Salomon, 1987). PCC oxidation (Pedrosa, Andres, & Iglesias, 2001) of **12** yielded the aldehyde **13** (66% yield), δ_{CHO} 9.80, which upon reaction with hydroxylamine hydrochloride gave a mixture of *Z*/*E* oximes (**14**) (89% yield) with a 4:1 ratio according to the integration of the olefinic proton signal (δ 6.65, 1H, t, J = 5.2 Hz; δ 7.35, 0.25H, t) in the ^{1}H NMR spectrum. Catalytic hydrogenation of the *Z*-oxime product (**14a**), obtained by recrystallization from isopropanol, under the same condition as described for the preparation of **7**, gave 3-(3,4-dimethoxyphenyl)propylamine·HCl (**15**) (86% yield) (Scheme 2).

4-(3,4-Dimethoxyphenyl)butylamine (**19**) was prepared starting from the aryl propanal **13**. Reaction of **13** with malonic acid in the presence of pyridine and piperidine (Knoevenagel-Doebner reaction) (Duarte et al., 2004) gave a mixture of β,γ- and α,β-unsaturated pentenoic acids (**16a**/**b**) with a ratio 3:1, determined by integration of the olefinic proton signals in the ^{1}H NMR spectrum, δ 7.07 (dt, J = 15.6, 6.7 Hz, H-3) and 5.81 (br. d, J = 15.6 Hz, H-2) (**16b**); δ 5.75–5.56 (m, 2H, H-3,4) (**16a**). Catalytic hydrogenation of **16a**/**b** afforded the pentanoic acid **17** (96% yield over two-step reaction from **13**), which through Schmidt reaction (sodium azide/ sulfuric acid) (Werner & Casanova, Werner & Casanova Jr., 1967) yielded the sulfonated derivative (**18**) of the desired 4-(3,4-dimethoxyphenyl)butylamine (**19**) (47% yield). Structure of **18** was elucidated based on analysis of the ^{1}H NMR spectrum, showing two singlets for the *para*-aryl protons (δ 7.49 & 6.84) and the HRMS (ESI) data, showing $[M+H]^+$ at m/z 312.0878 for the molecular formula $C_{12}H_{19}NNaO_5S$ (calcd. 312.0876). Desulfonation of **18** with 50% sulfuric acid under reflux (Ehrenfeld & Puterbaugh, 1932) gave the sulfate salt of 4-(3,4-dimethoxyphenyl)butylamine (**19**) (91% yield). Esterification of **16a**/**b** with ethanol/sulfuric acid (cat.) yielded the ethyl ester **20a**/**b** (95% yield), which under similar conditions for the preparation of the amine **15** afforded 5-(3,4-dimethoxyphenyl)pentylamine · HCl (**25**) (Scheme 2).

Coupling of the naphthoic acid **4** with various arylalkanamines (**7**, **8**, **15**, **19**, and **25**), catalyzed by 1-ethyl-3-(3′-dimethylamino)carbodiimide (EDC) and 1-hydroxybenzotriazole (HOB) (Takahashi & Miyazawa, 2011), afforded the amides **26**–**29** (81–90% yield), and **30** (37% yield), which were per-*O*-demethylated by boron tribromide to give the target *N*-arylalkanyl 2-naphthamides **Xa-e** (51–99% yield). Acetylation of **Xc** with acetic anhydride in pyridine yielded the peracetylated **31** (Scheme 3).

3.3 | In vitro anti-xanthine oxidase activity of target compounds and correlation with molecular docking

The inhibitory activity against xanthine oxidase (XO) of the prepared *N*-arylalkanyl 2-naphthamides (**Xa-e**) was assayed (Khan et al., 2008) and the result was shown in Table 1. Among these, **Xb-d** showed better inhibitory activity against XO ($IC_{50} \sim 13$ μM), comparable to the positive control allopurinol (IC_{50} 22.1 μM) but weaker than **II** (IC_{50} 7.4 μM). **Xa** and **Xe**, however, showed weaker inhibitory activity. The in vitro assay result indicated that the activity of *N*-arylalkanyl 2-naphthamides increased apparently as the length of the alkyl-linker extends from n = 1 to n = 2, and roughly the same from n = 2 to n = 4, but decreased as n = 5. This bioassay results correlated well with the molecular docking scores as indicated above (Table 1), verifying the applicability of the virtual screening on this established XO template.

3.4 | In silico evaluation of target compounds against xanthine oxidase

According to our previous research, the caffeoyl residue of netpetoidin B (**II**) was inserted into the binding site of XO to form one H-bond to Arg880, and hence the styrenyl catechol residue was oriented to form one H-bond to Ser876. Additional two H-bonds were formed between the styrenyl catechol residue to His875 and Glu879, both of which were close to the binding site (Figure 3c) (Ho et al., 2020). As compounds **Xa-e** were derived from **II**, further investigation of the binding behavior of **Xa-e** to the XO active site

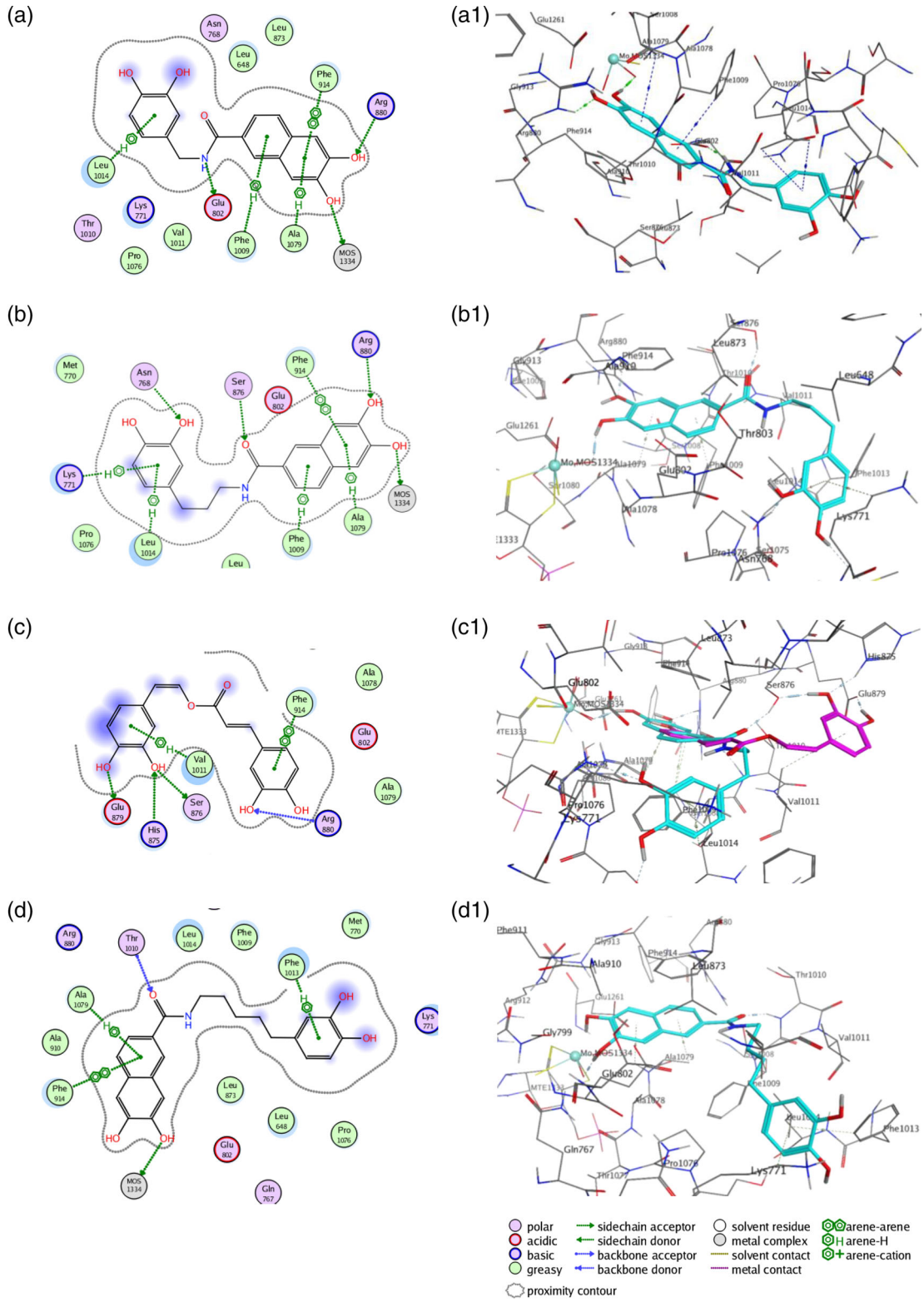

FIGURE 3 Molecular modeling of XO with compounds **Xa,c&e** and **II** in the presence of Mo cofactor. Docking results, depicted as two-dimensional (**Xa**: a; **xc**: b; **II**: c; **Xe**: d) and three-dimensional conformation (**Xa**: a1; **Xc**: b1; **II** (magenta)/**Xc** (blue): c1; **Xe**: d1), are shown in the left and right panel, respectively

was performed and the results were revealed in Figure 3 (**Xa**,**c&e**) and Supporting Information (**Xb&d**), where the dihydroxynaphthyl moiety was positioned in the molybdenum center.

The interactions of **Xa-d** to XO bore some similarities, including one H-bond with Arg880, one π–π interaction with Phe914, and one π–H interaction with Ala1079 in the 2,3-dihydroxynaphthyl moiety to

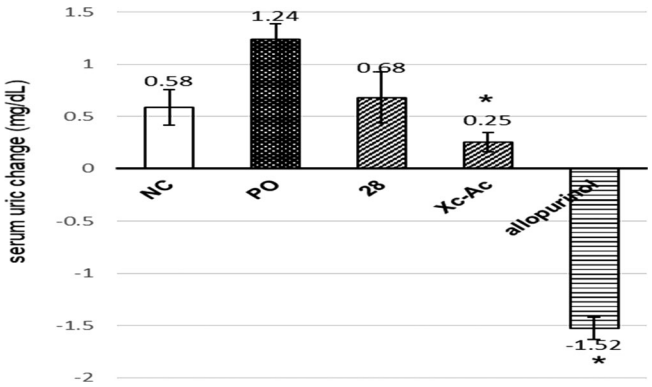

FIGURE 4 Effect of oral administration of **28** (30 mg/kg) and **Xc-Ac** (**31**; 40 mg/kg) on serum uric acid after i.p. administration of potassium oxonate (PO, 250 mg/kg) in male ICR mice (the *y*-axis represent as serum uric acid change level after 7 days). Data are the mean ± *SEM* for four animals; NC: normal control group, PO: potassium oxonate induced hyperuricemia group; **p* < .01 comparing with PO; for PO, *p* = .059 comparing with NC

the binding site of XO, and one H-bond to the cofactor Mo. Additional π–π interaction was observed from this moiety in **Xc** and **Xd** to Phe1009. **Xa** with a shorter aliphatic linker (*n* = 1) let the catechol moiety reach only the edge of salicylate binding pocket, thus showing weaker binding affinity. Compounds with longer aliphatic linkers like **Xc** (*n* = 3) and **Xd** (*n* = 4) made the catechol moiety pose nearby the salicylate binding site pocket and showed one π-H interaction with Leu1014 and one H-bond with Asn768, thus having better binding affinity. An extra H-bond interaction of the catechol moiety in **Xc** to Lys771, located nearby the binding site, stabilized the fitting conformation, leading to slightly higher binding affinity score than **Xd** (Δ*G* −17.66 vs. −17.13 Kcal/mol) (Table 1).

The interactions of **Xe** (*n* = 5) to XO, showing one H-bond to the binding site and one H-bond to the cofactor Mo (Figure 3d/d_1), were quite different from those of **Xa-d**, thus showing weak bonding affinity (Table 1).

The docking comparisons between **II** and **Xc**, the latter of which showing the highest docking score among **Xa-e** to XO, indicated the common interactions including two H-bonds with Arg880 and Ser876 in the binding site. In **II**, the *cis*-styryl catechol served as proton donor to form H-bond with Ser876 (Figure 3c/c_1), contributing Δ*G* − 3.4 Kcal/mol. Nevertheless, it is the naphthoyl amide carbon in **Xc** serving as proton acceptor (Figure 3b/b_1), contributing Δ*G* −1.3 Kcal/mol only. This explained why **II** had better binding score to XO than **Xc** (Δ*G* −19.32 vs. −17.66 Kcal/mol).

3.5 | Evaluation of the in vivo efficacy in hyperuricemia mice model

Xc, one of the most active compounds against XO, was subjected to evaluate anti-hyperuricemic efficacy in potassium oxonate induced hyperuricemia mice model (Kong et al., 2004; Wu et al., 2014). As the two catechol moieties in **Xc** might cause stability problem, peracetylation was performed to give the acetylated prodrug **Xc-Ac** (**31**). The permethylated **Xc** (**28**) was also assayed in vivo to clarify the role of these catechol moieties in anti-hyperuricemic efficacy. The change of serum uric level after 7 days' drug treatment was shown in Figure 4. The serum uric level was found 60% and 80% reduction for **31** treated group (0.25 mg/dL) in comparison to the normal control group (0.58 mg/dL) and the potassium oxonate induced hyperuricemia model group (1.24 mg/dL), the latter comparison being statistically significant (*p* = .0014, <.01), The compound **28** treated group showed that serum uric acid level was declined to almost the level of normal group but without statistical significance. However, both compounds were less effective than allopurinol. The docking score of **31** is much less than **Xc** and **28**. However, in vivo study revealed that it was more potent than **28**, indicating **Xc-Ac (31)** to be hydrolyzed to the parent compound **Xc** to achieve the uric acid lowering effect. The in vivo efficacy of **31**, however, might not reflect that of **Xc**, partly attributable to its poor solubility. The poor solubility of **28** also caused its IC_{50} value against XO unavailable. Nevertheless, molecular docking result showed that the binding potential of **28** was lower than **Xc**, correlating well with the in vivo result.

Kidney is the main route for uric acid excretion and therefore the uricosuric agents are considered effective to lower serum uric acid (SUA) level. However, to achieve such effect, their systemic absorption and transport to renal tubules are necessary and these might cause systemic adverse effect including liver and kidney damage. The approved XOIs also have similar disadvantage (Robinson & Dalbeth, 2015). Recently some evidences emphasize that intestinal tract is an important organ for lowering SUA in rats. Highly expressed XO on upper intestinal tract was contributed to the level of uric acid in the intestine tissue and serum (Yun et al., 2017). Compound **Xc** in this study blocks the uric acid synthesis at least in the intestine to achieve SUA lowering effect. Whether the poor solubility of these prepared target compounds might hamper their absorption by the intestine, resulting less systemic side effects, requires further investigation.

4 | CONCLUSION

In the present study, an established XO molecular docking template was applied to virtually screen *N*-arylalkanyl naphthamides designed from 1,4-benzodioxane type neolignans. The scaffold of such target compounds has been identified as new class of XO inhibitors form both in vitro and in vivo assays. Compounds **Xc** and **Xd** showed most potent XO inhibitory effects, comparable to allopurinol. The in vivo efficacy of the **Xc** prodrug on hyperuricemia mice model showed the reduction of blood uric acid level as compared with the vehicle control. *N*-Arylalkanyl 2-naphthamides could be thought as new lead for further development of XO inhibitors.

ACKNOWLEDGMENT

This work was supported by the Ministry of Science and Technology, Taiwan under the grants MOST 103-2320-B-002-011-MY3.

CONFLICT OF INTEREST

The authors declare no potential conflict of interests.

AUTHOR CONTRIBUTIONS

Ching-Ting Lin was involved in synthesis and bioactivity analysis and wrote the manuscript draft. Sheau Ling Ho was involved in XO template production, target compound design, data collection and refinement for structural studies, and wrote/edited manuscript. Shoei-Sheng Lee co-designed target compounds, supervised the experiments, conceived the project and integrated all data and completed the manuscript.

DATA AVAILABILITY STATEMENT

Data has been attached as Supporting Information and in the manuscript.

ORCID

Shoei-Sheng Lee https://orcid.org/0000-0002-6628-2448

REFERENCES

Cao, H. N., Pauff, J. M., & Hille, R. (2014). X-ray crystal structure of a xanthine oxidase complex with the flavonoid inhibitor quercetin. *Journal of Natural Products*, *77*, 1693–1699.

Chen, S. L., Zhang, T. J., Wang, J., Wang, F. Y., Niu, H. D., Wu, C. F., & Wang, S. J. (2015). Synthesis and evaluation of 1-hydroxy/methoxy-4-methyl-2-phenyl-1*H*-imidazole-5-carboxylic acid derivatives as non-purine xanthine oxidase inhibitors. *European Journal of Medicinal Chemistry*, *103*, 343–353.

Cos, P., Ying, L., Calomme, M., Hu, J. P., Cimanga, K., Van Poel, B., … Vanden Berghe, D. (1998). Structure-activity relationship and classification of flavonoids as inhibitors of xanthine oxidase and superoxide scavengers. *Journal of Natural Products*, *61*, 71–76.

Duarte, C. D., Verli, H., de Araujo-Junior, J. X., de Medeiros, I. A., Barreiro, E. J., & Fraga, C. A. M. (2004). New optimized piperamide analogues with potent in vivo hypotensive properties. *European Journal of Pharmaceutical Sciences*, *23*, 363–369.

Ehrenfeld, L., & Puterbaugh, M. (1932). *O*-Nitroaniline. *Organic Syntheses Collective Volumes*, *1*, 388–389.

Enroth, C., Eger, B. T., Okamoto, K., Nishino, T., Nishino, T., & Pai, E. F. (2000). Crystal structures of bovine milk xanthine dehydrogenase and xanthine oxidase: Structure-based mechanism of conversion. *National Academy of Sciences of the United States of America*, *97*, 10723−−10728.

Goksu, S., Kazaz, C., Sutbeyaz, Y., & Secen, H. (2003). A concise synthesis of 2-amino-1,2,3,4-tetrahydronaphthalene-6,7-diol ('6,7-ADTN') from naphthalene-2,3-diol. *Helvetica Chimica Acta*, *86*, 3310–3313.

Halgren, T. A. (1996). Merck molecular force field. 1. Basis, form, scope, parameterization, and performance of MMFF94. *Journal of Computational Chemistry*, *17*, 490–519.

Hille, R. (2006). Structure and function of xanthine oxidoreductase. *European Journal of Inorganic Chemistry*, *2006*(10), 1913–1926.

Ho, S. L., Tsai, S.-F., Lin, C.-T., Kim, H.-R., & Lee, S.-S. (2020). Validation of in silico docking analysis of oligophenylpropanoids to xanthine oxidase by correlation with in vitro bioassay and its application to Phlorotannins. *Journal of Drug Design and Medicinal Chemistry*, *6*(1), 1–6.

Ingebretsen, O. C., Borgen, J., & Farstad, M. (1982). Uric acid determinations: Reversed-phase liquid chromatography with ultraviolet detection compared with kinetic and equilibrium adaptations of the uricase method. *Clinical Chemistry*, *28*, 496–498.

Khan, W. N., Ali, I., Gul, R., & Choudhary, M. I. (2008). Xanthine oxidase inhibiting compounds from *Ranunculus repens*. *Chemistry of Natural Compounds*, *44*, 95–97.

Kong, L. D., Yang, C., Ge, F., Wang, H. D., & Guo, Y. S. A. (2004). Chinese herbal medicine Ermiao wan reduces serum uric acid level and inhibits liver xanthine dehydrogenase and xanthine oxidase in mice. *Journal of Ethnopharmacology*, *93*, 325−−330.

Kumar, R., Darpan, S. S., & Singh, R. (2011). Xanthine oxidase inhibitors: A patent survey. *Expert Opinion on Therapeutic Patents*, *21*, 1071–1108.

Lal, K., Ghosh, S., & Salomon, R. G. (1987). Hydroxyl-directed regioselective momodemethylation of polymethoxyarenes. *Journal of Organic Chemistry*, *52*, 1072–1078.

Lin, H. C., Tsai, S. H., Chen, C. S., Chang, Y. C., Lee, C. M., Lai, Z. Y., & Lin, C. M. (2008). Structure–activity relationship of coumarin derivatives on xanthine oxidase-inhibiting and free radical-scavenging activities. *Biochemical Pharmacology*, *75*, 1416–1425.

Pacher, P., Nivorozhkin, A., & Szabo, C. (2006). Therapeutic effects of xanthine oxidase inhibitors: Renaissance half a century after the discovery of allopurinol. *Pharmacological Reviews*, *58*, 87–114.

Pauff, J. M., & Hille, R. (2009). Inhibition studies of bovine xanthine oxidase by luteolin, silibinin, quercetin, and curcumin. *Journal of Natural Products*, *72*, 725–731.

Pedrosa, R., Andres, C., & Iglesias, J. M. (2001). A novel straightforward synthesis of enantiopure tetrahydroisoquinoline alkaloids. *Journal of Organic Chemistry*, *66*, 243–250.

Robinson, P. C., & Dalbeth, N. (2015). Advances in pharmacotherapy for the treatment of gout. *Expert Opinion on Pharmacotherapy*, *16*, 533–546.

Rock, K. L., Kataoka, H., & Lai, J. J. (2013). Uric acid as a danger signal in gout and its comorbidities. *Nature Review Rheumatology*, *9*, 13–23.

Saito, D., Kisen, T., Kumagai, M., & Ohta, K. (2018). Synthesis, structure-activity relationships, and mechanistic studies of 5-arylazo-tropolone derivatives as novel xanthine oxidase (XO) inhibitors. *Bioorganic & Medicinal Chemistry*, *26*, 536–542.

Silva, M. P., Mira, L., Lima, J., & Manso, C. F. (1996). Kinetics of the inhibition of xanthine dehydrogenase and of the reversible and irreversible forms of xanthine oxidase by silibinin and bendazac. *Environmental Toxicology and Pharmacology*, *1*, 279–284.

Soni, A., Rehman, A., Naik, K., Dastidar, S., Alam, M. S., Ray, A., Chaira, T., Shah, V., Palle, V. P., Cliffe, I. A., & Sattigeri, V. J. (2013). Synthesis and evaluation of 4,5-dihydro-5-methylisoxazolin-5-carboxamide derivatives as VLA-4 antagonists. *Bioorganic & Medicinal Chemistry Letters*, *23*, 1482–1485.

Takahashi, H., Matsumoto, K., Ueda, M., Miyake, Y., & Fukuyama, Y. (2002). Biomimetic syntheses of neurotrophic americanol a and isoamericanol a by horseradish peroxidase (HRP) catalyzed oxidative coupling. *Heterocycles*, *56*, 245−−256.

Takahashi, T., & Miyazawa, M. (2011). Synthesis and structure-activity relationships of phenylpropanoid amides of serotonin on tyrosinase inhibition. *Bioorganic & Medicinal Chemistry Letters*, *21*, 1983–1986.

Tsai, S. F., & Lee, S. S. (2014). Neolignans as xanthine oxidase inhibitors from *Hyptis rhomboides*. *Phytochemistry*, *101*, 121–127.

Tsou, H. R., Liu, X., Birnberg, G., Kaplan, J., Otteng, M., Tran, T., Kutterer, K., Tang, Z., Suayan, R., Zask, A., Ravi, M., Bretz, A., Grillo, M., McGinnis, J. P., Rabindran, S. K., Ayral-Kaloustian, S., & Mansour, T. S. (2009). Discovery of 4-(benzylaminomethylene)isoquinoline-1,3-(2*H*,4*H*)-diones and 4-(pyridylmethyl)aminomethylene isoquinoline-1,3-(2*H*,4*H*)-diones as potent and selective inhibitors of the cyclin-dependent kinase 4. *Journal of Medicinal Chemistry*, *52*, 2289–2310.

Werner, N. W., & Casanova, J., Jr. (1967). Cyclobutylamine. *Organic Syntheses Collective Volumes*, *47*, 28.

Wu, X. H., Ruan, J. L., Zhang, J., Wang, S. Q., & Zhang, Y. W. (2014). Pallidifloside D, a saponin glycoside constituent from Smilax riparia, resist to hyperuricemia based on URAT1 and GLUT9 in hyperuricemic mice. *Journal of Ethnopharmacology*, *157*, 201–205.

Yun, Y., Yin, H., Gao, Z., Li, Y., Gao, T., Duan, J., Yang, R., Dong, X., Zhang, L., & Duan, W. (2017). Intestinal tract is an important organ for lowering serum uric acid in rats. *PLoS One*, *12*, e0190194.

Zhang, T. J., Li, S. Y., Yuan, W. Y., Zhang, Y., & Meng, F. H. (2018). Design, synthesis, and molecular docking studies of *N*-(9,10-anthraquinone-2-carbonyl)amino acid derivatives as xanthine oxidase inhibitors. *Chemical Biology & Drug Design*, *91*, 893–901.

Zhang, T. J., Lv, Y. Y., Lei, Y., Liu, D., Feng, Y., Zhao, J. X., … Wang, S. J. (2018). Design, synthesis and biological evaluation of 1-hydroxy-2-phenyl-4-pyridyl-1*H*-imidazole derivatives as xanthine oxidase inhibitors. *European Journal of Medicinal Chemistry*, *146*, 668–677.

SUPPORTING INFORMATION

Additional supporting information may be found online in the Supporting Information section at the end of this article.

How to cite this article: Ho SL, Lin C-T, Lee S-S. In silico design and synthesis of N-arylalkanyl 2-naphthamides as a new class of non-purine xanthine oxidase inhibitors. *Drug Dev Res*. 2021;1–13. https://doi.org/10.1002/ddr.21782